Contribution from the Chemistry Department,
University of Virginia, Charlottesville, Virginia 22901

Chiroptical Luminescence Spectra of UO_2^{2+} in Cubic $Na[UO_2(CH_3COO)_3]$ Crystals

Diane M. Moran, David H. Metcalf, and F. S. Richardson*

Received August 6, 1991

Steady-state chiroptical luminescence measurements are reported for cubic crystals of $Na[UO_2(CH_3COO)_3]$. These crystals belong to the enantiomorphic space group $P2_13$, with four molecules per unit cell, and each $UO_2(CH_3COO)_3^-$ coordination unit has a *chiral* tris-bidentate chelate structure of C_3 symmetry. The $UO_2O'_6$ coordination clusters (where O′ denotes an acetate oxygen donor atom) also have *chiral* structures of C_3 point-group symmetry, but they deviate only slightly from an *achiral* D_{3h} symmetry. The luminescence observed for $Na[UO_2(CH_3COO)_3]$ is assigned to transitions that originate from the lowest electronic excited state (Π_g) of UO_2^{2+} and terminate on the ground electronic state (Σ_g^+). At least two types of UO_2^{2+} species contribute to this luminescence, but the luminescence spectra can be analyzed in terms of separate *majority* species (or bulk site) contributions and *minority* species (or defect site) contributions. The luminescence spectra show zero-phonon origin lines, one-phonon false-origin lines, and vibronic progressions in the symmetric stretching mode (ν_s) of UO_2^{2+}. The false-origin lines and the progressions based on these lines are essentially unpolarized. However, the origin lines and their progressions exhibit a very large degree of circular polarization, with emission dissymmetry factors of $g_{em} = 1.31$ (majority species) and $g_{em} = 0.96$ (minority species). The circularly polarized luminescence results for $\Sigma_g^+ \leftarrow \Pi_g$ emission are compared to circular dichroism results for $\Sigma_g^+ \rightarrow \Pi_g$ absorption, and the distribution of $\Sigma_g^+ \leftrightarrow \Pi_g$ electronic rotatory strength among origin and vibronic lines is discussed within the context of vibronic optical activity theory.

Introduction

Cubic crystals of sodium uranyl acetate, $Na[UO_2(CH_3COO)_3]$, are of special interest in the study of solid-state natural optical activity. These crystals belong to the enantiomorphic space group $P2_13$, with four molecules per unit cell.[1] Each UO_2^{2+} ion is coordinated to three acetate ions via bidentate chelation modes, with the mean plane of the six acetate donor atoms (oxygens) being nearly perpendicular to the O–U–O^{2+} axis. However, each of the UO_2^{2+}–acetate chelate rings is slightly canted out of this equatorial plane, with one donor atom of each ring lying ≈0.04 Å above the plane and the other lying ≈0.04 Å below the plane. Furthermore, the U–O bond distances for these two donor atoms are slightly different (2.51 versus 2.47 Å). Thus, the point-group symmetry of each $UO_2O'_6$ cluster in the crystal (where O′ denotes an acetate donor atom) is exactly C_3. The site symmetry of the uranium atoms in the crystal structure is also C_3.[1]

Sodium uranyl acetate crystallizes spontaneously from solution into one of its enantiomorphic forms, and individual crystals exhibit "natural" chiroptical properties. It is one of the very few optically active materials having a *cubic* crystal structure and one of the few that is formed entirely from *achiral* molecular subunits. The sole sources of chiroptical effects in its structure are (1) the inherent chirality of *each* $UO_2O'_6$ coordination cluster due to the helical canting of the three UO_2^{2+}–acetate chelate rings, and (2) the noncentrosymmetric spatial arrangement of the four coordination clusters in each unit cell of the crystal. The latter is likely to be important only for spectroscopic transitions involving strongly coupled "collective" excitations spanning all the chromophores in a unit cell (i.e., cases where spatial dispersion and strong exciton coupling effects cannot be ignored). For the *intra*-valence-shell electronic transitions localized on individual UO_2^{2+} chromophores, the chiroptical properties can most likely be accounted for entirely in terms of single-site $UO_2O'_6$ chirality. Intersite couplings between the spectroscopic states involved in these transitions are expected to be weak.

The first experimental studies of optical activity in $Na[UO_2(CH_3COO)_3]$ crystals were reported by Samoilov in 1948.[2] In that report it was claimed that certain fluorescent lines exhibited complete (perfect) circular polarization and that several absorption lines in the visible region of the spectrum were perfectly circular dichroic. These rather remarkable claims were later disputed by Brodin and Dovgii[3] and by Burkov et al.,[4] although these workers also reported absorption lines showing a high degree of circular dichroism. More recently, Denning et al.[5] have reported absorption and circular dichroism spectra of $Na[UO_2(CH_3COO)_3]$ at 10 K, and they observed several lines with large absorption dissymmetry $|\Delta\epsilon/\epsilon|$ values within the lowest-energy electronic transition region (between 21 050 and 21 900 cm^{-1}). This transition region is assigned to a $\Sigma_g^+ \rightarrow \Pi_g$ electronic excitation on the uranyl ion, and the strongly circular dichroic lines observed in this transition region are assigned to the electronic origin (zero-phonon) transition and to members of a vibronic progression in the totally symmetric stretching mode of the UO_2^{2+} ion. In the $\Sigma_g^+ \rightarrow \Pi_g$ transition region, absorption lines assigned to vibronically-induced false origins and to progressions based on these false origins do not exhibit a detectable circular dichroism.[5,6] Chowdhury and co-workers have carried out direction-dependent linear dichroism (LD)[7] and circular dichroism (CD)[8] measurements on $Na[UO_2(CH_3COO)_3]$ to assess the possible importance of electric quadrupole transition mechanisms in the observed optical properties. They find no evidence for electric quadrupole contributions to the $\Sigma_g^+ \rightarrow \Pi_g$ transition properties, but their results suggest that electric quadrupole contributions to the higher energy $\Sigma_g^+ \rightarrow \Delta_g$ transitions should not be ignored.

The $\Sigma_g^+ \leftarrow \Pi_g$ emission properties of $Na[UO_2(CH_3COO)_3]$ crystals have been investigated by a number of workers. Chan et al.[9] have reported emission spectra and emission decay kinetics measured over the 77–295 K temperature range, Denning and co-workers[10] have reported time-resolved luminescence measurements and emission excitation spectra obtained at 4.2 K, Flint and Sharma[11] have reported luminescence spectra obtained under variable-temperature conditions, and Murata et al.[12] have reported circularly polarized luminescence (CPL) measurements obtained at 4.2 and 77 K. The variable-temperature luminescence measurements show no evidence for structural phase transitions in $Na[UO_2(CH_3COO)_3]$, but these measurements and emission

* To whom correspondence should be addressed.

(1) Zachariasen, W. H.; Plettinger, H. A. *Acta Crystallogr.* **1959**, *12*, 526–530.
(2) Samoilov, B. N. *Zh. Eksp. Teor. Fiz.* **1948**, *18*, 1030–1040.
(3) Brodin, M. S.; Dovgii, Yu. O. *Opt. Spectrosc.* (*Engl. Transl.*) **1962**, *12*, 155–157.
(4) Burkov, V. I.; Krasilov, Yu. I.; Kizel, V. A.; Madii, V. A.; Semin, G. S. *Opt. Spectrosc.* (*Engl. Transl.*) **1975**, *39*, 397.
(5) Denning, R. G.; Foster, D. N. P.; Snellgrove, T. R.; Woodwark, D. R. *Mol. Phys.* **1979**, *37*, 1089–1107.
(6) Denning, R. G. In *Vibronic Processes in Inorganic Chemistry*; NATO ASI Series C: Mathematical and Physical Sciences 288; Flint, C. D., Ed.; Kluwer Academic Publishers: Dordrecht, The Netherlands, 1989; pp 111–137.
(7) Banerjee, A. K.; Chowdhury, M. *Chem. Phys. Lett.* **1987**, *139*, 421–425.
(8) Banerjee, A. K.; Karmaker, B.; Chowdhury, M. *Chem. Phys. Lett.* **1987**, *141*, 232–236.
(9) Chan, W. K.; Chun, K. H.; Lai, T. W.; Leung, A. F. *Can. J. Phys.* **1979**, *57*, 2045–2049.
(10) Denning, R. G.; Ironside, C. N.; Snellgrove, T. R.; Stone, P. J. *J. Chem. Soc., Dalton Trans.* **1982**, 1691–1697.
(11) Flint, C. D.; Sharma, P. *J. Chem. Soc., Faraday Trans. 2* **1983**, *79*, 317–321.
(12) Murata, K.; Yamazaki, Y.; Morita, M. *J. Lumin.* **1979**, *18/19*, 407–410.

0020-1669/92/1331-0819$03.00/0

excitation spectra give clear evidence for at least two major types of UO_2^{2+} emitting sites as well as a number of other minor sites that can act as energy traps.[10,11,13] Temperature-dependent, time-resolved emission measurements reveal facile energy transfer between the two major types of sites—designated as A and B by Denning.[10] At low temperatures ($T < 10$ K), the zero-phonon origin lines associated with emission from these two sites are located at 21 100 (A) and 21 132 cm^{-1} (B). The vibrational structures associated with the site A and site B emission spectra are quite similar with respect to the locations of one-phonon false-origin lines (relative to the true-origin lines) and the intensity distributions observed within vibronic progressions based on both the true- and false-origin lines (vide infra). Denning has proposed that the A and B sites are structurally identical with respect to the immediate coordination sphere of the uranyl ion and that the A sites are distinguished from the B sites only by some structural disorder among the sodium ions about the A sites.[10] He has further proposed that the *relative* abundance of the A sites is ca. 5%.

In the study reported here, steady-state chiroptical luminescence measurements were carried out on single crystals of $Na[UO_2(CH_3COO)_3]$ at temperatures between 6 and 298 K. Both *total luminescence* (TL) and *circularly polarized luminescence* (CPL) spectra were measured over the 470–640-nm wavelength range, and *emission dissymmetry factors* were determined for the most optically active (i.e., circularly polarized) emission lines observed in this spectral region. Following the standard practice in chiroptical luminescence studies,[14,15] we use the following definitions of TL intensity (I), CPL intensity (ΔI), and emission dissymmetry factor (g_{em}):

$$I(\bar{\nu}) = I_L(\bar{\nu}) + I_R(\bar{\nu}) \quad (1)$$

$$\Delta I(\bar{\nu}) = I_L(\bar{\nu}) - I_R(\bar{\nu}) \quad (2)$$

$$g_{em}(\bar{\nu}) = 2\Delta I(\bar{\nu})/I(\bar{\nu}) \quad (3)$$

Here $\bar{\nu}$ denotes emission wavenumber, and I_L and I_R denote intensities of the left (L) and right (R) circularly polarized components of the emitted light.

Murata et al.[12] have previously reported chiroptical luminescence measurements for $Na[UO_2(CH_3COO)_3]$ at 4.2 and 77 K, but their measurements were not sufficiently extensive to support a detailed analysis of the results. Our TL and CPL measurements span a much broader spectral range, and we report high-resolution absorption and CD measurements in the low-energy portion of the $\Sigma_g^+ \rightarrow \Pi_g$ transition region. These measurements are crucial for rationalizing the apparently anomalous TL, CPL, and emission dissymmetries observed in the origin lines of the A-site and B-site emission spectra (vide infra). Resolution of these anomalies permits separate evaluations of A-site versus B-site chiroptical activity (as gauged by emission dissymmetry factors), and it also permits the evaluation of Huang–Rhys parameters for the Σ_g^+ (ground) and Π_g (excited) electronic states of UO_2^{2+} in $Na[UO_2(CH_3COO)_3]$.

The $\Sigma_g^+ \leftarrow \Pi_g$ chiroptical luminescence spectra and emission dissymmetry data obtained in this study are entirely consistent with the chiroptical absorption properties observed for the $\Sigma_g^+ \rightarrow \Pi_g$ transition region.[5,6,16] In both absorption and emission, strong chiroptical activity is observed only in the zero-phonon lines (of the A and B site species) *and* in vibronic progressions built on those origin lines with vibrational quanta of the UO_2^{2+} symmetric stretching mode (ν_s). Vibronically-induced false origin lines and progressions built on these false origins appear prominently in the absorption and emission spectra, but they exhibit vanishingly small absorption and emission dissymmetry factors. These observations suggest that the zero-phonon origin transitions (and their vibronic progressions in ν_s) have a predominantly *magnetic dipole* character, whereas the false-origin lines have essentially pure *electric dipole* character.[6] This is compatible with the inherent properties of the Σ_g^+ and Π_g electronic states of UO_2^{2+} (as described by Denning),[5,17] and with extant theories of molecular vibronic chiroptical activity (vide infra).[18-20]

In $Na[UO_2(CH_3COO)_3]$, crystal-field perturbations can mix the even-parity Σ_g^+ and Π_g electronic states of UO_2^{2+} with odd-parity states to produce *mixed-parity* states that transform as A (Σ_g^+ parentage) and E (Π_g parentage) irreducible representations in the C_3 point group (which reflects the symmetry of the crystal-field perturbations). Purely electronic (zero-phonon) optical transitions between these perturbed states, $A(\Sigma_g^+) \leftrightarrow E(\Pi_g)$, are both electric and magnetic dipole allowed by C_3 symmetry selection rules, and the electric dipole and magnetic dipole transition vectors will be polarized either parallel or antiparallel to one another. These properties satisfy the necessary conditions for chiroptical activity in the $A(\Sigma_g^+) \leftrightarrow E(\Pi_g)$ electronic transitions, as reflected in the following expression for transition rotatory strength

$$R_{AE} = \mathrm{Im}\,[\langle A|\hat{\mu}|E\rangle \cdot \langle E|\hat{\mathbf{m}}|A\rangle] \quad (4)$$

where Im stands for the imaginary part (of the quantity that follows), $\hat{\mu}$ and $\hat{\mathbf{m}}$ respectively denote electric and magnetic dipole moment (vector) operators, and a summation over the degenerate components of the $|E\rangle$ state vectors is implied. Transition rotatory strengths determine both the signs and intensities of CD and CPL lines observed in chiroptical spectra,[15] and the electronic rotatory strength given by eq 4 is applicable to CD and CPL observed in the zero-phonon lines *and* their vibronic progressions within the $A(\Sigma_g^+) \leftrightarrow E(\Pi_g)$ absorption and emission spectra. Both the electric and magnetic dipole transition vectors in eq 4 can reflect crystal-field effects, but only the electric dipole transition vector has *essential* dependence on the crystal-field perturbations. The unperturbed $\Sigma_g^+ \leftrightarrow \Pi_g$ transitions are magnetic dipole allowed.

Experimental Section

Optical quality single crystals of $Na[UO_2(CH_3COO)_3]$ were grown by slow evaporation of saturated aqueous solutions of the salt, slightly acidified with acetic acid. Variable-temperature absorption and emission measurements were carried out with the crystal sample mounted in the sample compartment of either an Air Products liquid-helium-transfer Heli-Trans refrigerator (with temperature control provided by an Air Products temperature controller, Model 3700) or a CTI-Cryogenics closed-cycle helium refrigerator (with temperature control provided by a Lake Shore Cryotronics temperature controller, Model DRC-70). The crystal was mounted on a one-piece copper mount using indium foil, and the copper mount was attached to the cold head of the refrigerator, with strips of indium providing a thermally conductive interface. All optical experiments were carried out using a 180° ("head-on") excitation-detection configuration, and both the front and rear faces of the crystal were polished prior to making measurements.

Steady-state *total luminescence* (TL) and *circularly polarized luminescence* (CPL) measurements were performed using instrumentation and methodology developed in our laboratory at the University of Virginia.[21,22] The 454.5-nm output of an argon ion laser (Coherent Innova 90-6) was used for emission excitation. This excitation falls in an absorption region assigned to overlapping $\Sigma_g^+ \rightarrow \Pi_g$ and $\Sigma_g^+ \rightarrow \Delta_g$ transition manifolds of the uranyl ion. The emission is dispersed with a high-resolution Spex 1400-II double monochromator with gratings blazed at 500 nm, and a red-sensitive EMI 9558 photomultiplier tube with associated photon-counting electronics is used to detect the emission intensity. Steady-state TL (I) and CPL (ΔI) spectra were measured over the 470–640-nm wavelength range (see eqs 1 and 2 for the definitions of the TL and CPL intensity observables, I and ΔI) at a spectral reso-

(13) Abramov, A. P.; Razumova, I. K. *Opt. Spectr.* **1975**, *38*, 565.
(14) (a) Richardson, F. S.; Riehl, J. P. *Chem. Rev.* **1977**, *77*, 773–791. (b) Riehl, J. P.; Richardson, F. S. *Chem. Rev.* **1986**, *86*, 1–16.
(15) Richardson, F. S. *J. Less-Common Met.* **1989**, *149*, 161–177.
(16) Palmer, R. A. Duke University, unpublished results.
(17) Denning, R. G.; Snellgrove, T. R.; Woodwark, D. R. *Mol. Phys.* **1979**, *37*, 1109–1143.
(18) Moffitt, W.; Moscowitz, A. *J. Chem. Phys.* **1959**, *30*, 648–660.
(19) (a) Weigang, O. E. *J. Chem. Phys.* **1965**, *43*, 3609–3618. (b) Harnung, S. E.; Ong, E. C.; Weigang, O. E. *J. Chem. Phys.* **1971**, *55*, 5711–5724. (c) Weigang, O. E.; Ong, E. C. *Tetrahedron* **1974**, *30*, 1783–1793.
(20) Richardson, F. S. In *Stereochemistry of Optically Active Transition Metal Compounds*; ACS Symposium Series 119; Douglas, B. E., Saito, Y., Eds., American Chemical Society: Washington, DC, 1980; Chapter 3.
(21) (a) Metcalf, D. H.; Snyder, S. W.; Demas, J. N.; Richardson, F. S. *J. Am. Chem. Soc.* **1990**, *112*, 5681–5695. (b) Metcalf, D. H.; Snyder, S. W.; Demas, J. N.; Richardson, F. S. *J. Phys. Chem.* **1990**, *94*, 7143–7153.
(22) Metcalf, D. H.; Cummings, W. J.; Richardson, F. S. Manuscript in preparation.

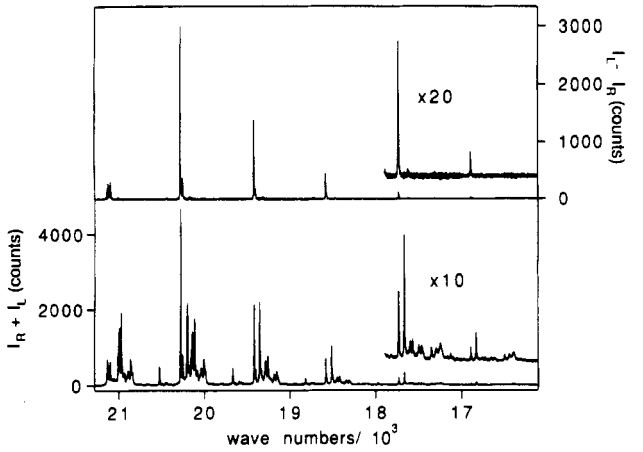

Figure 1. Survey CPL (top trace, $I_L - I_R$) and TL (bottom trace, $I_L + I_R$) spectra for a single crystal of $Na[UO_2(CH_3COO)_3]$ over the 21 300–16 100-cm^{-1} range. This spectral range covers the true- and false-origin lines of the UO_2^{2+} $\Sigma_g^+ \leftarrow \Pi_g$ electronic transition and the first five members of vibronic progressions in the symmetric UO_2^{2+} stretching mode. The crystal temperature was 6 K, the excitation wavelength was 454.5 nm, and the spectral resolution was 1 cm^{-1}.

lution of ca. 0.02 nm. Observed emission intensities were corrected for instrument response using procedures described in ref 23 and the fluorescence standard, quinine sulfate dihydrate. Integrated line intensities were determined by spectral deconvolution to combination Lorentzian–Gaussian line shapes using a Marquardt-based nonlinear least-squares-fitting algorithm.

Circular dichroism/absorption measurements were conducted using the same monochromator/detection system (as described above for emission measurements) in a single-beam transmission configuration. The output from a 500-W xenon arc lamp (PTI A5000 housing) was passed through a high-throughput, low-resolution monochromator (Spex Mini-Mate) and focused through a polarizer and photoelastic modulator (Hinds PEM-80) combination to produce a circular-polarization-modulated beam. This beam was passed through the sample, and the transmitted radiation dispersed using the Spex 1400-II monochromator. Photoelastic modulator phase-sensitive photon-counting electronics were used to determine the transmission spectra relative to left and right circularly polarized light. These spectra were converted to absorbance $A = (A_L + A_R)/2$ and circular dichroism $\Delta A = (A_L - A_R)$ spectra (where A_L and A_R are decadic absorbances for left (L) and right (R) circularly polarized light) by correcting for the arc-lamp output profile and the dispersion characteristics of the monochromator.

Results and Analysis

Spectra. TL and CPL spectra measured over the 21 300–16 100-cm^{-1} range at a sample temperature of 6 K are shown in Figure 1. These spectra span the true- and false-origin lines of the uranyl $\Sigma_g^+ \leftarrow \Pi_g$ electronic transition *and* the first five members of vibronic progressions in the symmetric stretching mode (ν_s) of UO_2^{2+}. The 21 250–19 550-cm^{-1} regions of the spectra are shown in greater detail in Figure 2. The following spectral features are identified and labeled in Figure 2: A-site and B-site origin lines (labeled as *A* and *B*, respectively); the first member of the ν_s vibronic progression based on the B-site origin (labeled as *s*); and false-origin lines associated with the B-site and assigned to the UO_2^{2+} rocking (ν_r), bending (ν_b), and asymmetric stretching (ν_a) modes, (labeled as *r*, *b*, and *a*, respectively, in the figure). The origin lines are located at 21 132 (*B*) and 21 100 cm^{-1} (*A*), which are in close agreement with results reported previously by Denning et al.[10] and by Flint and Sharma.[11] The false-origin lines assigned to B-site emission are displaced from the 21 132-cm^{-1} (*B*) origin line by 240 (ν_r), 272 (ν_b), and 933 cm^{-1} (ν_a), and the first member of the $B - n\nu_s$ progression is located at a displacement frequency of 856 cm^{-1}. The first member of the $A - n\nu_s$ progression occurs at a displacement frequency of 850 cm^{-1}.

Many of the unlabeled features of the TL spectra shown in Figure 2 have been discussed, and in some cases characterized

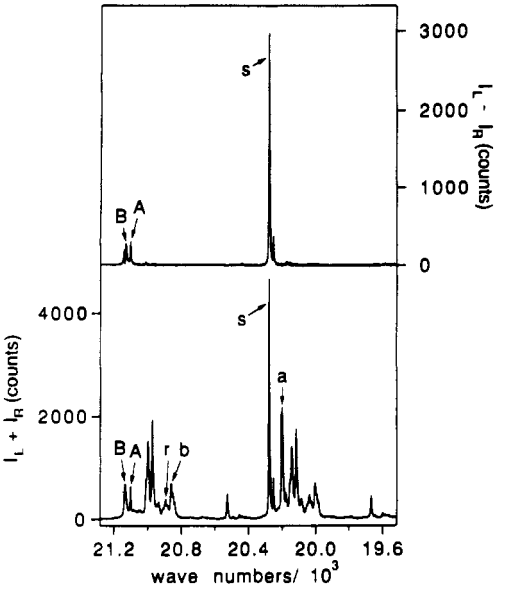

Figure 2. Detail of the true- and false-origin regions and the members of the first vibronic progression region shown in Figure 1. Experimental conditions are the same as given in the caption to Figure 1.

Table I. Emission Dissymmetry Factors Measured for the $B - n\nu_s$ and $A - n\nu_s$ Lines in the CPL/TL Spectra

	$B - n\nu_s$		$A - n\nu_s$	
n	$\bar{\nu}$, cm^{-1} [a]	$g_{em}(B)$ [b]	$\bar{\nu}$, cm^{-1} [a]	$g_{em}(A)$ [b]
0 (origin)	21 132	n.d.	21100	0.90
1	20 276	1.28	20250	0.97
2	19 421	1.35	19402	1.01
3	18 577	1.30	18564	n.d.
4	17 729	1.40	n.d.	n.d.
5	16 887	1.23	n.d.	n.d.

[a] Transition wavenumber, $1/\lambda$(vac). n.d. ≡ not determined. [b] Defined according to eq 3 of the text. n.d. ≡ not determined.

and assigned, by Denning, Flint, and co-workers.[10,11] Neither these features nor those associated with the ν_r, ν_b, and ν_a false-origin transitions (cited above) have detectable counterparts in the CPL spectra, and we shall not focus further attention on them *except* to rationalize their lack of chiroptical activity (vide infra). We shall focus instead on the *A* and *B* origin lines and their $A - n\nu_s$ and $B - n\nu_s$ progressions, which contain essentially all the chiroptical activity of the uranyl $\Sigma_g^+ \leftarrow \Pi_g$ transition manifold.

Emission dissymmetry factors (g_{em}) measured for various members of the $A - n\nu_s$ and $B - n\nu_s$ progressions are given in Table I. These dissymmetry factors, defined according to eq 3, were determined from CPL/TL data obtained at 6 K. Emission dissymmetry in the B-site origin transition could not be determined due to complications arising from self-absorption effects (vide infra). The CPL lines associated with members of the $A - n\nu_s$ progression were too weak to permit determination of g_{em} values for $n > 2$. The data in Table I yield *average* A-site and B-site emission dissymmetry factors of $g_{em}(A) = 0.96$ and $g_{em}(B) = 1.31$. The relative intensities of A-site versus B-site TL and CPL lines change when sample temperature is incrementally varied from 6 to 298 K. However, the CPL/TL intensity ratios ($\Delta I/I$) do *not* change with temperature, and the $g_{em}(A)$ and $g_{em}(B)$ values appear to be invariant to temperature changes.

The TL and CPL spectra exhibit several peculiar characteristics in the lines assigned to the A-site and B-site origin transitions. From the spectra shown in Figure 2 we note the following: (1) the *B*-origin line is broader than the *A*-origin line in the TL spectrum, (2) the relative intensities of the *B*- versus *A*-origin lines are dramatically different from those observed in the $n \neq 0$ members of the $B - n\nu_s$ and $A - n\nu_s$ progressions, and (3) the CPL spectrum shows structure in the *B*-origin, but not the *A*-origin, region. Following Denning et al.,[10] we attribute the greater breadth of the *B*-origin line to the presence of multiple "B-like"

(23) Velapoldi, R. A.; Mielenz, K. D. *NBS Special Publication 260-64*; U.S. Government Printing Office: Washington, DC, 1980.

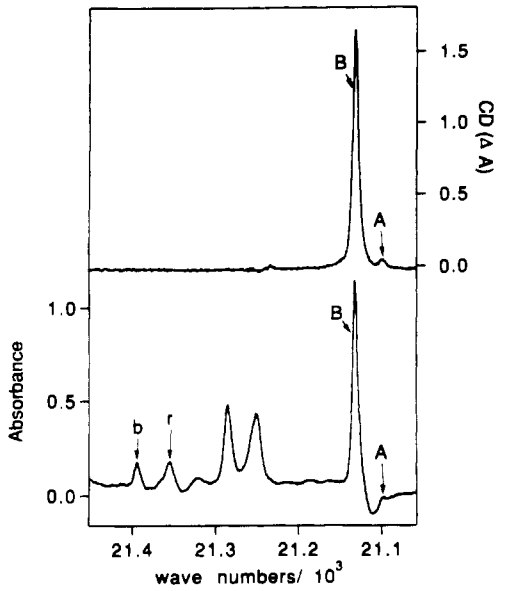

Figure 3. Circular dichroism (top, $\Delta A = A_L - A_R$) and absorbance (bottom, $A = (A_L + A_R)/2$) for $Na[UO_2(CH_3COO)_3]$ over the 21 060–21 450-cm^{-1} range. A and B labels refer to the origin lines of the $\Sigma_g^+ \rightarrow \Pi_g$ transition for UO_2^{2+} ions in A and B sites, respectively, and the *b* and *r* labels refer to $B + n\nu_r$ and $B + n\nu_b$ vibronic transitions. The crystal temperature was 10 K, and the spectral resolution was 5 cm^{-1}.

sites in the crystal. The reduced *B* versus *A* intensity ratio observed in the origin transitions (relative to the ratios observed in the respective ν_s progressions) can be attributed to self-absorption of *B*-origin emission. Self-absorption of this emission was also observed in the work of Denning, Flint, and coworkers.[10,11] The structure observed in the *B*-origin transition region of the CPL spectrum (between 21 150 and 21 110 cm^{-1}) is not replicated in any of the $B - n\nu_s$ vibronic lines of the CPL spectrum. A possible explanation for this structure in terms of *circular dichroic* self-absorption is given below.

Circular dichroism (CD) and absorption spectra measured over the 21 060–21 450-cm^{-1} range are shown in Figure 3. The *A*- and *B*-origin lines of the $\Sigma_g^+ \rightarrow \Pi_g$ transition manifold are identified in the spectra, and the false-origin lines assigned to $B + n\nu_r$ and $B + n\nu_b$ vibronic transitions are also marked (with *r* and *b* labels, respectively). The negative-absorbance dip observed in the absorption spectrum on the lower-frequency side of the *B*-origin line is caused by B-site emission. In the CD spectrum, the *B*-origin line is centered at 21 136 cm^{-1} and the *A* origin line is located at 21 100 cm^{-1}. Absorption dissymmetry in the *B*-origin line is $g_{abs} = \Delta A/A \approx 1.4$, which is close to the average value measured for g_{em}(B), 1.31. A comparison of the CPL/TL spectra (Figure 2) with the CD/absorption spectra (Figure 3) in the *A*- and *B*-origin regions reveals (1) the attenuation of B-site emission attributable to self-absorption (vide supra), and (2) the appearance of structure in the CPL but *not* in the CD spectra within the *B*-origin transition region.

An enlarged view of the TL and CPL spectra in the *B*-origin transition region (21 150–21 110 cm^{-1}) is shown in Figure 4. Note that the TL band has a flattened top and some shoulder features and the CPL spectrum exhibits two clearly resolved maxima (and the hint of some shoulder features) within the TL bandwidth. The CPL features span a slightly broader frequency range than does the *B*-origin CD band shown in Figure 3, and the centroid of the *B*-origin emission (located at 21 132 cm^{-1}) is displaced from the CD band centroid (at 21 136 cm^{-1}) by 4 cm^{-1}. The dip between the two peaks in the CPL spectrum is nearly coincident with the CD band maximum. These observations suggest that the dip (or hole) in the CPL spectrum may be attributed to *narrow-line, circular dichroic* self-absorption, whereas the overall TL intensity attenuation (and band flattening) includes broader-line, unpolarized self-absorption processes. Circular dichroic self-absorption within the *B*-origin transition region will lead to a *decrease* in the

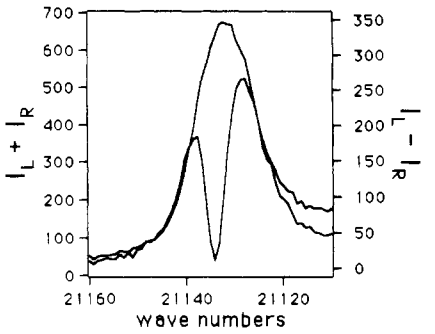

Figure 4. Detail of the *B*-origin region from Figures 1 and 2. The CPL trace ($I_L - I_R$) is that trace with the "dip" in it. Experimental conditions are the same as given in the caption to Figure 1.

intensity of that circular polarization of light that is preferentially emitted during the transition since that same polarization of light will be preferentially absorbed (by the *reverse* transition). The depth of the negative dip will be dependent on the relative number of emitting and absorbing sites within the crystal and thus will be dependent on such experimental conditions as excitation power and excitation–emission geometry. Spectral results from this region are fully consistent with these observations.

The TL spectrum shown in Figure 4 has a flattened top, and it also exhibits a barely discernible shallow dip at 21 136 cm^{-1}, which corresponds to the location of the "hole" in the CPL spectrum. This would suggest a physical model in which a distribution of B-like absorber species contributes to the self-absorption of total (polarized *and* unpolarized) emission intensity, whereas only a subpopulation of this distribution contributes to circular dichroic self-absorption of circularly polarized emission. The observed CPL spectrum indicates that the entire distribution of B-like species gives circularly polarized emission but that circular dichroic self-absorption of this emission occurs only over a relatively narrow frequency range. Finally, we point out again that the "hole" observed in the *B*-origin CPL spectrum is not replicated in any of the CPL lines of the $B - n\nu_s$ vibronic progression. This gives further evidence that the hole reflects circular dichroic self-absorption *rather* than oppositely signed CPL contributions from emitting species with opposite structural chiralities.

It was noted earlier that the relative intensities of A-site versus B-site emission lines are temperature dependent, but the g_{em}(A) *and* g_{em}(B) dissymmetry factors are independent of temperature. In agreement with results reported by Flint and Sharma,[11] we find that A-site emission *increases* rapidly with *decreasing* sample temperature. This most likely reflects the temperature dependence of electronic energy-transfer processes between the A and B sites.[10,11] The TL spectrum we recorded at a nominal sample temperature of 6 K (see Figures 1 and 2) is essentially identical to the 4.2 K spectrum reported by Denning et al.[10] *except* that our A- versus B-site emission intensity ratios are smaller. It is possible that the effective (internal) crystal temperature in our experiments was slightly higher than the temperature (6 K) measured at the crystal surface.

Vibronic Intensity Distributions. The TL and CPL intensity distributions observed in the $B - n\nu_s$ progression and TL intensity distributions observed in several $(B - \nu_p) - n\nu_s$ progressions (where $(B - \nu_p)$ denotes a false origin associated with a *promoting* mode ν_p) were used to determine Huang–Rhys parameters (*S*) for both the Σ_g^+ (ground) and Π_g (excited) electronic states. In performing these parametric analyses of intensity distributions, we ignored anharmonicities in both the ground-state and excited-state ν_s vibrations, and we used the values 855 and 723 cm^{-1} for the fundamental frequency of ν_s in the ground and excited[5] states, respectively. The Huang–Rhys parameters obtained from our intensity data fits are $S(\Sigma_g^+) = 0.98$ and $S(\Pi_g) = 0.83$. These parameter values imply a difference of $\approx$0.07 Å between the ground-state (Σ_g^+) and excited-state (Π_g) U–O bond lengths in UO_2^{2+}.

The emission intensity distribution calculated for a progression in ν_s is shown in Figure 5. This distribution closely matches that

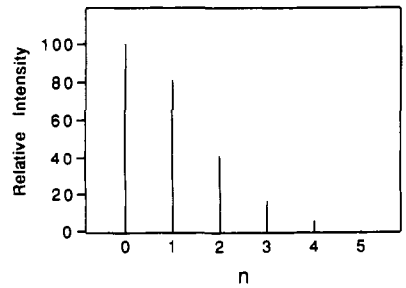

Figure 5. Emission intensity distribution calculated for a progression in the UO_2^{2+} symmetric stretching mode. See text for details.

observed in the experimental spectra (see Figure 1) when self-absorption of the origin line ($n = 0$) emission is taken into account. The calculated and observed intensity distributions are most easily compared for the relatively sparce CPL spectra.

Chiroptical Activity. For steady-state chiroptical luminescence measurements on an optically *isotropic* emitting sample, the CPL intensity (per unit solid angle) associated with a transition F ← I is given by

$$\Delta I(\bar{\nu}) = \left(\frac{32\pi^3 c}{3}\right)\frac{\bar{\chi}\bar{N}_I\bar{\nu}^4[\rho_{FI}(\bar{\nu})]R_{FI}}{g_I} \tag{5}$$

where $\bar{N}_I$ is the number of emitting species in level I under the steady-state excitation-emission conditions of the experiment, g_I denotes the electronic (or vibronic) degeneracy of level I, $\bar{\chi}$ is a factor dependent on the refractivity of the bulk sample medium, $\rho_{FI}(\bar{\nu})$ is a unit-normalized line-shape function centered at the transition frequency $\bar{\nu}_{FI}$, and R_{FI} is a transition *rotatory strength*. The emission dissymmetry factor for this transition is given by

$$g_{em} = \frac{2\Delta I(\bar{\nu})}{I(\bar{\nu})} = \frac{4\bar{\chi}R_{FI}}{\chi D_{FI}^{(e)} + \chi' D_{FI}^{(m)}} \tag{6}$$

where $\Delta I(\bar{\nu})$ and $I(\bar{\nu})$ are assumed to have identical lineshapes (each centered at $\bar{\nu}_{FI}$), $D_{FI}^{(e)}$ and $D_{FI}^{(m)}$ are the electric (e) and magnetic (m) dipole strengths of the transition, and χ and χ' are correction factors for bulk sample refractivity effects. In principle, transition rotatory strengths can be determined from *integrated* CPL line intensities according to the expression

$$R_{FI} = \left(\frac{3g_I}{32\pi^3 c\bar{\chi}\bar{N}_I}\right)\int \frac{\Delta I(\bar{\nu})}{\bar{\nu}^4}\,d\bar{\nu} \tag{7}$$

where the integration is over the F ← I transition line width. However, quantitative evaluation of eq 7 is generally precluded by difficulties in determining the value of $\bar{N}_I$. On the other hand, emission dissymmetry factors can be determined directly and accurately from CPL/TL ($\Delta I/I$) measurements.

Now we consider a *vibronic* transition between the *i*th vibrational level of electronic state I and the *f*th vibrational level of electronic state F. In the adiabatic Born–Oppenheimer approximation, the vibronic wavefunctions for the initial (Ii) and final (Ff) states of this transition may be written as $\Psi_I(r,Q)\Phi_{Ii}(Q)$ and $\Psi_F(r,Q')\Phi_{Ff}(Q')$, where r denotes electron coordinates, Q denotes nuclear vibrational coordinates in electronic state I, and Q' denotes nuclear vibrational coordinates in electronic state F. The rotatory strength of the Ff ← Ii vibronic transition is given by[20]

$$R_{Ff,Ii} = \text{Im}\,[\mathbf{P}_{Ff,Ii}\cdot\mathbf{M}_{Ii,Ff}] \tag{8}$$

where

$$\mathbf{P}_{Ff,Ii} = \langle\Psi_F(r,Q')\Phi_{Ff}(Q')|\hat{\mu}(r)|\Psi_I(r,Q)\Phi_{Ii}(Q)\rangle \tag{9}$$

$$\mathbf{M}_{Ii,Ff} = \langle\Psi_I(r,Q)\Phi_{Ii}(Q)|\hat{\mathbf{m}}(r)|\Psi_F(r,Q')\Phi_{Ff}(Q')\rangle \tag{10}$$

and $\hat{\mu}$ and $\hat{\mathbf{m}}$ are electric and magnetic dipole moment operators (dependent only on electron coordinates). In what follows, it will be convenient to reexpress the vibronic rotatory strength as

$$R_{Ff,Ii} = \text{Im}\,[\langle\Phi_{Ff}(Q')|\mathbf{P}_{FI}|\Phi_{Ii}(Q)\rangle\cdot\langle\Phi_{Ii}(Q)|\mathbf{M}_{IF}|\Phi_{Ff}(Q')\rangle] \tag{11}$$

where

$$\mathbf{P}_{FI} = \langle\Psi_F(r,Q')|\hat{\mu}(r)|\Psi_I(r,Q)\rangle_r \tag{12}$$

$$\mathbf{M}_{IF} = \langle\Psi_I(r,Q)|\hat{\mathbf{m}}(r)|\Psi_F(r,Q')\rangle_r \tag{13}$$

The matrix elements in eqs 12 and 13 are evaluated only over the electron coordinates (r), and the $\mathbf{P}_{FI}$ and $\mathbf{M}_{IF}$ transition moments retain a functional dependence on the nuclear coordinates (Q and Q'). The matrix elements in eq 11 are evaluated over the nuclear coordinates. If either the initial (Ii) or final (Ff) vibronic level of the transition is degenerate, the expressions given above must be augmented by summations over the degenerate states.

Following previous work,[20] we define Q and Q' in terms of symmetrized normal coordinate sets $\{Q_\nu\}$ and $\{Q'_\nu\}$, and expand both $\mathbf{P}_{FI}$ and $\mathbf{M}_{IF}$ as Taylor series in $\{Q_\nu\}$ about the equilibrium nuclear configuration (for the electronic state I). Truncation of these expansions after the linear terms gives the expressions

$$\mathbf{P}_{FI} = \mathbf{P}^\circ_{FI} + \sum_\alpha\left(\frac{\partial\mathbf{P}_{FI}}{\partial Q_\alpha}\right)_\circ Q_\alpha \tag{14}$$

$$\mathbf{M}_{IF} = \mathbf{M}^\circ_{IF} + \sum_\beta\left(\frac{\partial\mathbf{M}_{IF}}{\partial Q_\beta}\right)_\circ Q_\beta \tag{15}$$

where each summation is over $\{Q_\nu\}$, and each quantity with a superscript *or* subscript ∘ is evaluated at the equilibrium values of $\{Q_\nu\}$. Substitution of eqs 14 and 15 into eq 11 yields

$$\begin{aligned}R_{Ff,Ii} = {}& \text{Im}\,(\mathbf{P}^\circ_{FI}\cdot\mathbf{M}^\circ_{IF})|\langle\Phi_{Ff}(Q')|\Phi_{Ii}(Q)\rangle|^2 + \\ & \text{Im}\sum_\alpha(\mathbf{P}'_{FI,\alpha}\cdot\mathbf{M}^\circ_{IF})\langle\Phi_{Ff}(Q')|Q_\alpha|\Phi_{Ii}(Q)\rangle\langle\Phi_{Ii}(Q)|\Phi_{Ff}(Q')\rangle + \\ & \text{Im}\sum_\beta(\mathbf{P}^\circ_{FI}\cdot\mathbf{M}'_{IF,\beta})\langle\Phi_{Ff}(Q')|\Phi_{Ii}(Q)\rangle\langle\Phi_{Ii}(Q)|Q_\beta|\Phi_{Ff}(Q')\rangle + \\ & \text{Im}\sum_\alpha\sum_\beta(\mathbf{P}'_{FI,\alpha}\cdot\mathbf{M}'_{IF,\beta})\langle\Phi_{Ff}(Q')|Q_\alpha|\Phi_{Ii}(Q)\rangle\langle\Phi_{Ii}(Q)|Q_\beta|\Phi_{Ff}(Q')\rangle\end{aligned} \tag{16}$$

where $\mathbf{P}'_{FI,\alpha}$ and $\mathbf{M}'_{IF,\beta}$ denote the partial derivatives shown in eqs 14 and 15, respectively.

All of the emissive transitions examined in the present study originate from the ground vibrational level of an excited $E(\Pi_g)$ electronic state of UO_2^{2+} in $Na[UO_2(CH_3COO)_3]$, and they terminate on the ground and excited vibrational levels of the $A(\Sigma_g^+)$ ground electronic state. The $E(\Pi_g)$ and $A(\Sigma_g^+)$ notation indicates state symmetry in the C_3 point group (and in the $D_{\infty h}$ group). In applications of eq 16 to these transitions, we use the following notational identities: E0 ≡ Ii and Af ≡ Ff. If it is assumed that the $E(\Pi_g)$ and $A(\Sigma_g^+)$ electronic states reflect strong $D_{\infty h}$ parentage and relatively weak crystal-field perturbations (of C_3 symmetry), then one may expect that $|\mathbf{M}^\circ_{EA}| \gg |\mathbf{M}'_{EA,\beta}|$, but that $|\mathbf{P}^\circ_{AE}| \approx |\mathbf{P}'_{AE,\alpha}|$, for the electronic transition moments in eq 16. On the basis of these expectations, eq 16 may be reduced to the following form in our consideration of Af ← E0 transition rotatory strengths:

$$\begin{aligned}R_{Af,E0} = {}& \text{Im}\,(\mathbf{P}^\circ_{AE}\cdot\mathbf{M}^\circ_{EA})|\langle\Phi_{Af}(Q')|\Phi_{E0}(Q)\rangle|^2 + \\ & \text{Im}\sum_\alpha(\mathbf{P}'_{AE}\cdot\mathbf{M}^\circ_{EA})\langle\Phi_{Af}(Q')|Q_\alpha|\Phi_{E0}(Q)\rangle\langle\Phi_{E0}(Q)|\Phi_{Af}(Q')\rangle\end{aligned} \tag{17}$$

The first term in eq 17 applies to the zero-phonon (*origin*) transition, A0 ← E0, and to vibronic progressions (in totally symmetric modes) based on this origin transition. The second term applies to vibronically-induced *false-origin* transitions, and to progressions based on these false-origin transitions, but this term will vanish if the equilibrium nuclear configurations in the ground (A) and excited (E) electronic states have identical symmetry.

All of the CPL observed in the $A(\Sigma_g^+)$ ← $E(\Pi_g)$ emission spectrum of UO_2^{2+} in $Na[UO_2(CH_3COO)_3]$ is assigned to Af ← E0 transitions in which $f \equiv n\nu_s$ (where $n\nu_s$ represents $n = 0, 1, \ldots$; quanta of the totally symmetric stretching mode of UO_2^{2+}), and the rotatory strengths of these transitions are given by the first term of eq 17. The electronic part of these vibronic rotatory strengths is identical to our earlier eq 4, and the vibrational part

may be expressed in terms of the ground-state Huang–Rhys parameter $S(\Sigma_g^+)$ to obtain

$$R_{Af,E0} = \mathrm{Im}\,[\langle A|\hat{\mu}|E\rangle\cdot\langle E|\hat{m}|A\rangle]\frac{e^{-S}S^n}{n!} \qquad (18)$$

where $f \equiv n\nu_s$ (vide supra). The dissymmetry factors for the $Af \leftarrow E0$ transitions ($f \equiv n\nu_s$) are not modulated by n, and they are given by

$$g_{em} = \frac{4\bar{\chi}\ \mathrm{Im}\,[\langle A|\hat{\mu}|E\rangle\cdot\langle E|\hat{m}|A\rangle]}{\chi|\langle A|\hat{\mu}|E\rangle|^2 + \chi'|\langle E|\hat{m}|A\rangle|^2} \qquad (19)$$

(see eq 6).

Discussion

The chiroptical properties of a molecular system are extraordinarily sensitive to the details of stereochemical and electronic structure.[14,15,19,20,24-26] The CPL spectra and emission dissymmetry factors measured for $Na[UO_2(CH_3COO)_3]$ show several interesting facets of chiroptical activity in this system. *First*, the emission dissymmetry data reveal a difference in the degree (but not the handedness) of structural chirality around the B-site (majority) versus A-site (minority) emitting species. The signs of the $g_{em}(B)$ and $g_{em}(A)$ dissymmetry factors are the same, but the magnitude of $g_{em}(B)$ is ca. 35% greater than the magnitude of $g_{em}(A)$. *Second*, a comparison of absorption and emission dissymmetries in the $\Sigma_g^+ \rightarrow \Pi_g$ CD/absorption and $\Sigma_g^+ \leftarrow \Pi_g$ CPL/emission spectra shows that $g_{abs}(B)$ is ca. 7% larger in magnitude than $g_{em}(B)$. This indicates a small difference between ground-state (Σ_g^+) versus excited-state (Π_g) structural chirality around the B-site absorbers and emitters. *Third*, essentially all of the chiroptical activity in the $\Sigma_g^+ \leftarrow \Pi_g$ emission spectrum is observed in the zero-phonon (*origin*) transitions *and* in vibronic progressions built on these origins with vibrational quanta of the UO_2^{2+} symmetric stretching mode (ν_s). Emission lines assigned to one-phonon (*false-origin*) transitions and to progressions built on these false origins do not exhibit significant circular polarization. These observations demonstrate that the rotatory strength of the uranyl $\Sigma_g^+ \leftarrow \Pi_g$ electronic transition derives almost entirely from *static* crystal-field perturbations. However, the substantial (but unpolarized) emission intensity observed in false-origin lines (and in progressions based on these lines) shows that *dynamic*, phonon-mediated interactions make significant contributions to the total dipole strength of the $\Sigma_g^+ \leftarrow \Pi_g$ transition.

The results obtained in this study are generally compatible with the work of Denning and co-workers,[5,6,10] and most of our notation and references to uranyl electronic states and vibrational modes conform to Denning's prescriptions. We have focused primarily on the circularly polarized components of the $\Sigma_g^+ \leftarrow \Pi_g$ emission spectra and have given considerably less attention to the unpolarized parts of these spectra. The latter have been addressed in more detail by Denning et al.[10] and by Flint and Sharma.[11] Our emission dissymmetry data might call into question Denning's proposal regarding structural differences between the A-site and B-site chromophores (or luminophores) in $Na[UO_2(CH_3COO)_3]$. Denning proposed that the A and B sites are structurally identical with respect to the immediate coordination sphere of the uranyl ion (i.e., the structure of $UO_2(CH_3COO)_3^-$ is the same in the two sites) but that the A sites are distinguished from the B sites by structural disorder among the Na^+ ions around the A sites.[10] The 35% difference we find between the $g_{em}(A)$ and $g_{em}(B)$ dissymmetry factors suggests structural differences between the chiral $UO_2(CH_3COO)_3^-$ complexes in the two sites.

In the X-ray crystallographic structure reported for cubic $Na[UO_2(CH_3COO)_3]$ at room temperature,[1] the $UO_2(CH_3COO)_3^-$ complexes have C_3 point-group symmetry and the $UO_2O'_6$ coordination cluster in these complexes also has C_3 symmetry. The *mean* plane of the six acetate donor atoms (O′) is perpendicular to the $O–U–O^{2+}$ axis, but each of the three UO_2^{2+}–acetate (bidentate) chelate rings is slightly canted out of this equatorial plane. One donor atom of each acetate ligand is located ≈0.04 Å above the plane and the other is located ≈−0.04 Å below the plane. Furthermore, the U–O′ bond distances for these two donor atoms are slightly different (2.51 versus 2.47 Å). The uranyl moiety is linear, but its U–O bond distances are slightly asymmetric (1.72 versus 1.70 Å). If this asymmetry in UO_2^{2+} is ignored *and* if the differences among the U–O′ (acetate) bond distances are also ignored, the $UO_2O'_6$ coordination cluster would have trigonal dihedral (D_3) symmetry. If we further ignore the chelate ring cantings (and consider all six of the O′ donor atoms to be essentially coplanar), the $UO_2O'_6$ cluster would have D_{3h} symmetry and would be *achiral*. The extraordinarily strong chiroptical activity exhibited by UO_2^{2+} in $Na[UO_2(CH_3COO)_3]$ suggests that structural chirality *within* the $UO_2O'_6$ coordination cluster is very important. However, our chiroptical luminescence results indicate that a D_3 symmetry model is entirely adequate for rationalizing the observed CPL spectra and emission dissymmetry factors. We find no evidence for contributions from crystal-field interactions with an effective symmetry lower than D_3.

As described above, structural differentiation between D_3 versus C_3 symmetry in the $UO_2O'_6$ coordination cluster is based on differences among the U–O′ bond distances *and* on U–O bond asymmetry in the UO_2^{2+} moiety. The $UO_2O'_6$ vibrational modes that transform as the A_2 irreducible representation (irrep) under symmetry operations of the D_3 point group will transform as the totally symmetric A irrep in the C_3 point group. Among these vibrational modes is the $O–U–O^{2+}$ asymmetric stretching mode (ν_a). If these modes had significant $A(C_3)$ character, one would expect to see some of the $\Sigma_g^+ \leftarrow \Pi_g$ electronic rotatory strength (see eq 4) distributed into vibronic transitions assigned to them. Emission lines assigned to *origin* − ν_a and *origin* − ($\nu_a + n\nu_s$) vibronic transitions are seen prominently in the TL spectra of Figures 1 and 2, but they are not observed in the CPL spectra. Little or no rotatory strength is distributed into these transitions, and the ν_a vibrational mode appears to retain its non totally symmetric character (A_2 in the D_3 point group). This mode clearly promotes considerable electric dipole intensity in the $\Sigma_g^+ \leftarrow \Pi_g$ emission spectrum, but the electric dipole transition amplitudes associated with the ν_a-induced vibronic lines do not interfere *constructively* with resonant magnetic dipole transition amplitudes, and consequently, the ν_a-induced vibronic lines have no rotatory strength. With reference to our eq 17, both terms on the right-hand side will vanish for a vibronic transition $Ff \leftarrow I0$ in which f includes one or more quanta of a vibrational mode that is non totally symmetric (in both the I and F electronic states).

The strong chiroptical activity exhibited by the UO_2^{2+} electronic transitions in $Na[UO_2(CH_3COO)_3]$ is rather remarkable in view of the relatively small degree of structural chirality around the uranyl chromophore. The three UO_2^{2+}–acetate chelate rings deviate only slightly from a coplanar (achiral) geometry, and the degree of configurational chirality in this three-ring system is very small compared to that found in the structures of most optically-active lanthanide and transition-metal complexes. Detailed rationalization of electronic rotatory strengths in terms of crystal-field structure and interaction mechanisms is a formidable task in the study of *any* system, and the difficulties are compounded for systems in which the electronic state structure is strongly perturbed by crystal-field interactions, but in which the *chiral* components of the crystal field derive from subtle structural features. In this study, we do not attempt any rationalization of $\Sigma_g^+ \leftarrow \Pi_g$ electronic rotatory strength and emission dissymmetry in terms of crystal-field interaction details.

Conclusion

Sodium uranyl acetate crystals are relatively unique since they form cubic, enantiomorphic structures. In this study, we have measured chiroptical luminescence spectra from single crystals of $Na[UO_2(CH_3COO)_3]$. Luminescence from this system is

(24) Charney, E. *The Molecular Basis of Optical Activity: Optical Rotatory Dispersion and Circular Dichroism*; Wiley-Interscience: New York, 1979.
(25) Mason, S. F. *Molecular Optical Activity and the Chiral Discriminations*; Cambridge University Press: Cambridge, England, 1982.
(26) Barron, L. D. *Molecular Light Scattering and Optical Activity*; Cambridge University Press: Cambridge, England, 1982.

associated with UO_2^{2+} ions in majority and minority sites within the crystal. The luminescence is assigned to the $\Sigma_g^+ \leftarrow \Pi_g$ emissive transition origin, and to vibronic lines associated with this origin. Those vibronics associated with quanta of the symmetric stretching mode of UO_2^{2+} (ν_s) are strongly circularly polarized, while those that include quanta of asymmetric stretching or bending modes are essentially unpolarized. This behavior is rationalized in terms of a model of vibronic optical activity presented in the Results and Analysis section. Special consideration was given to the origin region of the $\Sigma_g^+ \leftarrow \Pi_g$ transition. The origin transition associated with the majority (B-site) UO_2^{2+} species shows interesting chiroptical behavior associated with circular dichroic self-absorption.

Acknowledgment. This work was supported by a grant from the National Science Foundation (CHE-8820180 to F.S.R.).

Registry No. $Na[UO_2(CH_3COO)_3]$, 17712-38-8.

Contribution from the Department of Chemistry,
North Dakota State University, Fargo, North Dakota 58105-5516

Hypercoordination in Group IV MH_5 and MH_5^- Systems

Marshall T. Carroll, Mark S. Gordon,* and Theresa L. Windus

Received July 17, 1991

The energetics and bonding of the group IV hypervalent MH_5 and MH_5^- D_{3h} structures (M = C, Si, Ge, Sn) are examined in this paper. Ab initio all-electron calculations are used to predict the energies and geometries of the systems. The resulting electron densities are analyzed using the topological theory of atoms in molecules. It is found that the anion energetically is more stable than the neutral radical for M = Si, Ge, and Sn but not for M = C. Further distinguishing carbon from the other members of the group is the fact that the CH bond mostly is of covalent character while the other MH bonds are mostly of ionic character. Scrutinizing difference density maps and atomic property changes reveals that, upon anion formation, the incoming electron density becomes preferentially accumulated in the nonbonded regions of the axial and, to a lesser extent, equatorial hydrogens.

Introduction

Hypervalent structures (compounds in which a central atom is apparently surrounded by more than the "normal" octet of electrons) are playing an increasingly important role in mechanistic interpretations of observed organosilicon chemistry. The simplest prototypical hypervalent silicon species is SiH_5^m, where m can be negative (anion), positive (cation), or neutral. Many theoretical papers have addressed the nature of the structure and bonding in SiH_5^-.[1-7] In a recent paper, Maitre and co-workers have used a valence bond model to account for the energy differences between SiH_5 and SiH_5^- (D_{3h} symmetry) and to explain the fact that the anion is a local minimum, while the neutral species apparently is not.[1] The essense of their analysis is that an ionic model is not sufficient for the description of SiH_5^-. This is in contrast to the ionic model that has been used to describe the electronic structure of SiH_4F^-.[8]

The SiH_5^- anion has been theoretically[1-7] and experimentally[9,10] characterized as a hypercoordinated species having D_{3h} symmetry. Even though the radical SiH_5 is predicted to be higher in energy than the anion,[1] the radical recently has been observed in an ESR spectrum,[11] as has its Group IV analogue GeH_5.[12] A theoretical investigation (at the unrestricted Moller-Plesset second-order perturbation level of theory at the restricted open-shell Hartree Fock geometry using a double-ζ basis set) has predicted that GeH_5 is an unstable transition state.[13] The lightest group IV hypervalent species, CH_5 and CH_5^-, have both been predicted to be unstable transition states with the radical energetically more stable than the anion.[6,10,14-16] To our knowledge, the corresponding tin systems, SnH_5 and SnH_5^-, have not yet been investigated.

In the present paper we use ab initio all-electron calculations to predict the structures and energies of group IV MH_5 and MH_5^- systems, for M = C, Si, Ge, and Sn. The theory of atoms in molecules[17] is employed to examine the nature of the bonding in these compounds.

The principal questions addressed in this paper are as follows:

(1) Does the fundamental nature of the M-H bond vary as a function of M, and if so, in what way?

(2) Why is SiH_5^- energetically more stable than SiH_5, while the opposite is true for M = C?

(3) In what manner does the total electron distribution change upon addition of an electron to the radical to form the anion?

(4) How do the properties of MH_4 change upon addition of H or H^- to form products?

Computational Approach

Ab initio all-electron calculations were performed using GAMESS.[18] Restricted Hartree-Fock (RHF) and restricted open-shell Hartree-Fock

(1) Maitre, P.; Volatron, F.; Hiberty, P. C.; Shaik, S. S. *Inorg. Chem.* **1990**, *29*, 3047.
(2) Sini, G.; Ohanessian, G.; Hiberty, P. C.; Shaik, S. S. *J. Am. Chem. Soc.* **1990**, *112*, 1407.
(3) Gordon, M. S.; Windus, T. L.; Burggraf, L. W.; Davis, L. P. *J. Am. Chem. Soc.* **1990**, *112*, 7167.
(4) Burggraf, L. W.; Davis, L. P.; Gordon, M. S. *Top. Phys. Organomet. Chem.* **1989**, *3*, 75.
(5) Reed, A. E.; Schleyer, P. v. R. *Chem. Phys. Lett.* **1987**, *133*, 553.
(6) Baybutt, P. *Mol. Phys.* **1975**, *29*, 389.
(7) Wilhite, D. L.; Spialter, L. *J. Am. Chem. Soc.* **1973**, *95*, 2100.
(8) Gronert, S.; Glaser, R.; Streitwieser, A. *J. Am. Chem. Soc.* **1989**, *111*, 3111.
(9) Hajdasz, D. J.; Squires, R. R. *J. Am. Chem. Soc.* **1986**, *108*, 3139.
(10) Payzant, J. D.; Tanaka, K.; Betovski, L. D.; Bohme, D. K. *J. Am. Chem. Soc.* **1976**, *98*, 894.
(11) Nakamura, K.; Masaki, N.; Sato, S.; Shimokoshi, K. *J. Chem. Phys.* **1985**, *83*, 4504.
(12) Nakamura, K.; Masaki, N.; Okamoto, M.; Sato, S.; Shimokoshi, K. *J. Chem. Phys.* **1987**, *86*, 4949.
(13) Moc, J.; Rudzinski, J. M.; Ratajczak, H. *Chem. Phys. Lett.* **1990**, *173*, 557.
(14) Dedieu, A.; Veillard, A. *J. Am. Chem. Soc.* **1972**, *94*, 6730.
(15) Morokuma, K.; Davis, R. E. *J. Am. Chem. Soc.* **1972**, *94*, 1060.
(16) Niblaeus, K.; Roos, B. O.; Siegbahn, P. E. M. *Chem. Phys.* **1977**, *26*, 59.
(17) Bader, R. F. W. *Atoms in Molecules: A Quantum Theory*; Clarendon Press: Oxford, England, 1990; and references therein.
(18) Schmidt, M. W.; Baldridge, K. K.; Boatz, J. A.; Jensen, J. H.; Koseki, S.; Gordon, M. S.; Nguyen, K. A.; Windus, T. L.; Elbert, S. T. *QCPE Bull.* **1990**, *10*, 52.

0020-1669/92/1331-0825$03.00/0